Glycolytic reprogramming in host response to *Borrelia burgdorferi*: A gene signature revealed by integrative bioinformatics analysis and machine learning

YAN DONG[1,2*], YANTONG CHEN[1*], YANSHUANG LUO[1], MENG LIU[1], CHAO SONG[3], XUESONG CHEN[3], FUSONG YANG[3], QINGYI LUO[4] and GUOZHONG ZHOU[2,3]

[1]Faculty of Life Science and Technology and The Affiliated Anning First People's Hospital, Kunming University of Science and Technology, Kunming, Yunnan 650302, P.R. China; [2]School of Basic Medical Sciences, Kunming University of Science and Technology, Kunming, Yunnan 650500, P.R. China; [3]Department of Pain Medicine, The Affiliated Anning First People's Hospital of Kunming University of Science and Technology, Kunming, Yunnan 650302, P.R. China; [4]Department of Ultrasound, Yanan Hospital of Kunming City, The Affiliated Hospital of Kunming Medical University, Kunming, Yunnan 650302, P.R. China

Received December 17, 2025; Accepted April 8, 2026

DOI: 10.3892/etm.2026.13182

Abstract. Lyme disease (LD), a multifaceted condition caused by *Borrelia burgdorferi* (Bb), remains poorly understood, particularly regarding metabolic pathways. This study aimed to evaluate the role of glycolysis-related genes (GRGs) in LD pathogenesis and identify key genes and mechanisms relevant to diagnosis and therapy. Differentially expressed GRGs were identified and further analyzed by correlation analysis and Gene Ontology and Kyoto Encyclopedia of Genes and Genomes enrichment analyses. Key genes were screened using least absolute shrinkage and selection operator (LASSO) and support vector machine-recursive feature elimination, followed by gene set enrichment analysis, gene set variation analysis and immune infiltration analysis using CIBERSORT. Diagnostic value was assessed by receiver operating characteristic and nomogram analyses, and a competing endogenous RNA network and protein-drug interaction predictions were constructed. The expression of key genes was further validated by reverse transcription-quantitative PCR (RT-qPCR) in Bb-infected THP-1 cells, and glucose and lactate concentrations in the culture supernatants were measured using commercial colorimetric assay kits. A total of 63 differentially expressed GRGs were identified. Of note, two key genes [lactate dehydrogenase A (LDHA) and thioredoxin (TXN)] exhibited a strong diagnostic performance. Immune infiltration analysis revealed that these genes were associated with regulatory T cells (r=0.33, P=0.05), gamma delta T cells (r=-0.34, P=0.042), CD4 memory resting T cells (r=-0.4, P=0.016) and monocytes (r=-0.36, P=0.03). The potential glycolysis-targeting drugs were predicted. RT-qPCR analysis revealed increased LDHA and TXN expression in Bb-infected THP-1 cells. In addition, Bb stimulation reduced extracellular glucose levels and increased lactate accumulation in culture supernatants. Overall, this integrative analysis revealed notable alterations in glycolytic genes during Bb infection, suggesting that dysregulation of glycolysis contributes to LD immunopathology. The identified key genes (LDHA and TXN) may serve as infection-related transcriptional response markers, offering insights into LD mechanisms and potential precision-based strategies.

Correspondence to: Dr Guozhong Zhou, Department of Pain Medicine, The Affiliated Anning First People's Hospital of Kunming University of Science and Technology, 2 Gangnan Road, Jinfang Street, Anning, Kunming, Yunnan 650302, P.R. China
E-mail: 20220247@kust.edu.cn

Dr Qingyi Luo, Department of Ultrasound, Yanan Hospital of Kunming City, The Affiliated Hospital of Kunming Medical University, 245 Renmin East Road, Panlong, Kunming, Yunnan 650302, P.R. China
E-mail: luoqingyi@kmmu.edu.cn

*Contributed equally

Key words: Borrelia burgdorferi, bioinformatics, potential drugs, glycolytic gene, immune cell infiltration, gene expression omnibus database

Introduction

Lyme disease (LD) is an infectious disease caused by the bacterium *Borrelia burgdorferi* (Bb), typically transmitted to humans through the bites of infected ticks (1). In recent years, the incidence of LD has significantly increased in the United States. According to estimates from the Centers for Disease Control and Prevention, the annual number of LD cases in the United States has increased to ~476,000, making it the most common tick-borne disease in the country (2). The clinical manifestations of LD are diverse, including skin rash, fever, headache, joint pain, and, in severe cases, complications affecting the nervous system, heart and joints (3).

Antibiotic treatment is currently the primary strategy for controlling LD. The current treatment strategy is effective in most cases; however, up to 17% of patients may still have some symptoms a year after treatment (4). Additionally, numerous reports have indicated that even after antibiotic treatment, Bb spirochetes can have targeted and persistent effects on the host immune system (5). Researchers have hypothesized that Bb uses various strategies to evade and suppress the host immune response, enabling it to persist within the human body for an extended period, leading to chronic infection and persistent symptoms. These strategies may include complement inhibition, antigen variation, extracellular matrix degradation and host immune dysregulation or suppression (6-8). Owing to the complexity and diversity of *Borrelia* species, the molecular mechanisms by which they modulate host immune responses remain poorly understood. Further identification of novel characteristic genes and virulence factors of Bb, as well as an in-depth exploration of their interactions with the host immune system, is of great significance for elucidating the pathogenesis of LD, finding new therapeutic targets and developing effective treatment strategies.

Glycolysis is a metabolic pathway that occurs in the cytoplasmic matrix in which a series of enzymatic reactions break down glucose molecules into pyruvate molecules, accompanied by the production of a small amount of ATP (9). Substantial evidence has suggested that glycolysis plays an important role in immune regulation. During the immune response, immune cells such as macrophages, dendritic cells and neutrophils rapidly activate glycolysis (10,11). This metabolic shift helps immune cells rapidly generate the energy and biosynthetic precursors required to support their immune functions, such as cell proliferation, differentiation, phagocytosis, cell migration and secretion of inflammatory factors (12,13). Excessive glycolysis can lead to an uncontrolled inflammatory response (14,15). Studies have shown that inhibiting glycolysis in immune cells can reduce inflammatory responses and modulate immune functions, which have potential applications in the treatment of autoimmune and chronic inflammatory diseases (16,17).

Changes in glycolysis have an important effect on the pathogenesis of LD. Bb infection can significantly enhance the glycolytic metabolism in host macrophages, leading to a weaker inflammatory response, reduced cytokine release, and increased survival and transmission of spirochetes within the host (18). Spirochetes also alter the protein composition of the saliva of the tick vector, upregulating the expression of glycolytic enzymes and providing more energy substrates for their own benefit, thereby promoting their colonization and replication at the tick bite site (19). Of note, inhibiting the glycolysis of host cells or directly inhibiting the key glycolytic enzymes (such as lactate dehydrogenase) of spirochetes can control the infection process, alleviate the inflammatory response and modulate host immune function, providing important clues for the development of new treatment strategies for LD (20,21). These findings reveal the critical role of glycolytic metabolism in the pathogenesis of LD and provide a new perspective for a deeper understanding of the disease mechanism.

In the present study, the differential expression of glycolysis-related genes (GRGs) and the immune profile of peripheral blood mononuclear cells (PBMCs) in individuals infected with Bb were systematically analyzed. The least absolute shrinkage and selection operator (LASSO) and support vector machine recursive feature elimination (SVM-RFE) machine learning methods were used to screened out risk characteristic genes, which were also validated in an external dataset, and it was found that these genes could be used to predict the occurrence of LD. Furthermore, a diagnostic predictive nomogram model was constructed, consistent clustering, immune infiltration and functional enrichment analyses of the screened risk characteristic genes were performed, and a competitive endogenous RNA (ceRNA) network and a drug-gene interaction regulatory network were constructed. The present results revealed the changes in GRG expression and immune profile in host PBMCs caused by Bb infection, providing a new perspective for understanding the pathogenesis of LD and potentially laying a theoretical foundation for the development of personalized treatment and immune regulation therapies for LD.

Methods

Data acquisition. The gene expression profiling datasets for peripheral blood samples stimulated with Bb, GSE42606 (GPL10558 platform) and GSE63085 (GPL11154 platform), were retrieved from the National Center for Biotechnology Information (NCBI) Gene Expression Omnibus (GEO) database (https://www.ncbi.nlm.nih.gov/geo/). Specifically, the GSE42606 dataset comprises 35 control samples (PBMCs from healthy donors were stimulated with RPMI control for 24 h) and 36 diseased samples (PBMCs from healthy donors were stimulated with Bb for 24 h). Although the data were derived from peripheral PBMCs rather than isolated macrophages, peripheral PBMCs contained a significant proportion of monocytes (macrophage precursors). The *ex vivo* stimulation of PBMCs by Bb effectively captured the early systemic activation and glycolytic shift of these innate immune cells, which is consistent with previous reports of enhanced macrophage glycolysis during Bb infection (18). The validation dataset (GSE63085) included 13 healthy control PBMC samples and 28 PBMC samples from patients with LD. The raw GEO data underwent normalization using R software (version 4.2.1; R Foundation for Statistical Computing; https://www.r-project.org/) and the limma function 'normalizeBetweenArrays'. A total of 200 GRGs wereobtained from the HALLMARK_GLYCOLYSIS gene set in the Molecular Signatures Database (MSigDB, v7.5.1; https://www.gsea-msigdb.org/gsea/msigdb). The gene list of GRGs is provided in Table SI. A comprehensive flowchart is shown in Fig. 1.

Identification of GRGs. Probe annotation was performed according to the corresponding platform annotation file to map probe IDs to gene symbols. For multiple probes mapping to the same gene symbol, expression values were averaged using the avereps() function in the limma package, so that each gene corresponded to a single expression value for downstream analysis. Differential expression analysis between normal and Bb-infected samples was then performed using the 'limma' package (22) with linear modeling and empirical Bayes moderation. P-values were adjusted using the Benjamini-Hochberg method, and differentially expressed

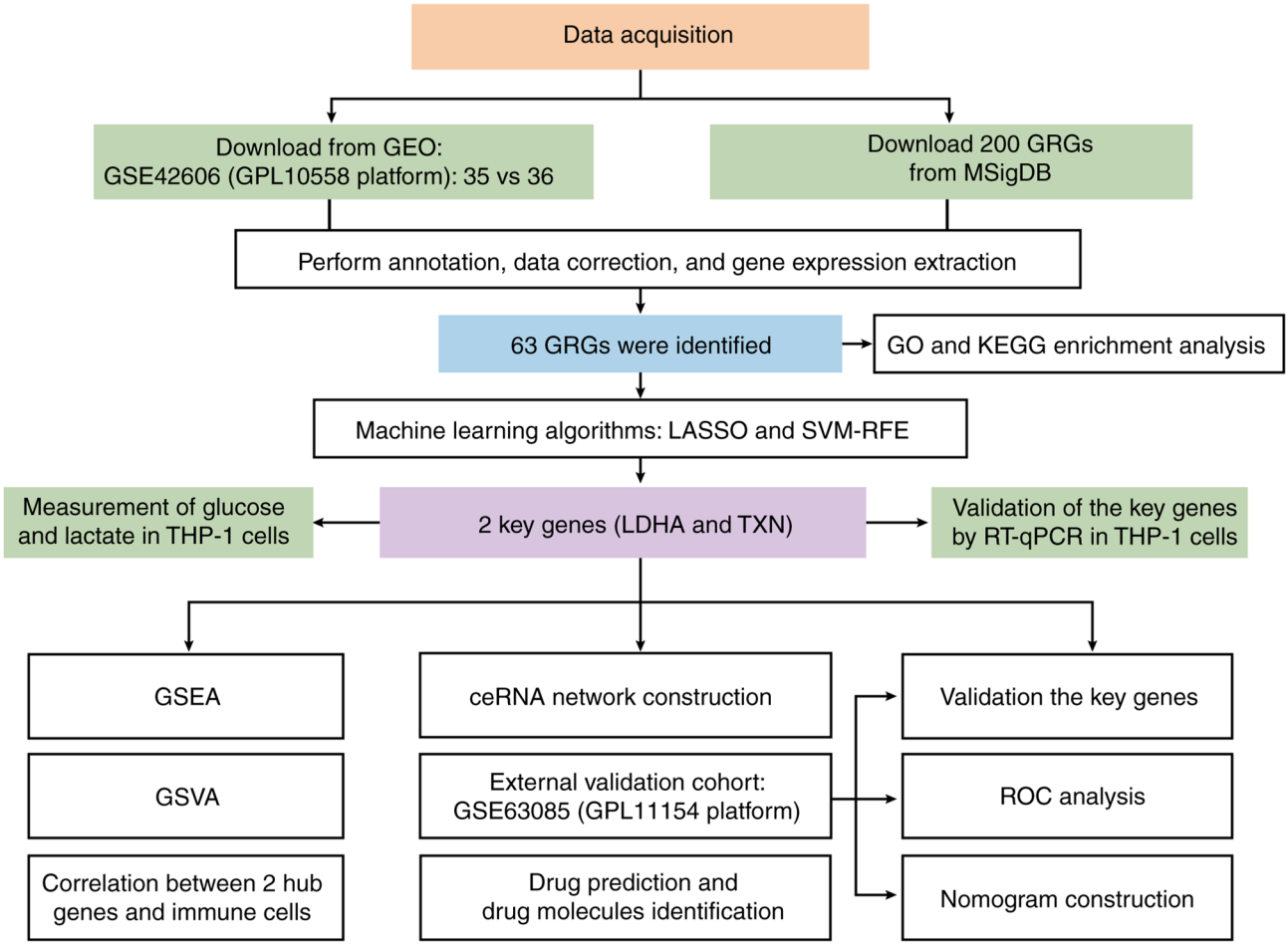

Figure 1. Flow chart for bioinformatics analysis of GRGs analysis in LD. GRGs, glycolysis-related genes; LD, Lyme disease; GEO, Gene Expression Omnibus; GO, Gene Ontology; KEGG, Kyoto Encyclopedia of Genes and Genomes; LASSO, Least Absolute Shrinkage and Selection Operator; SVM-RFE, Support Vector Machine-Recursive Feature Elimination; GSEA, Gene Set Enrichment Analysis; GSVA, Gene Set Variation Analysis; ceRNA, competing endogenous RNA; ROC, receiver operating characteristic; RT-qPCR, reverse transcription-quantitative PCR.

genes (DEGs) with an adjusted P<0.05 and log2 fold change (logFC) >0 were considered upregulated, while DEGs with logFC <0 were considered downregulated.

Correlation between the GRGs. The correlation coefficient for GRGs expression was computed and shown with the R package 'corrplot'.

Gene ontology (GO) and Kyoto encyclopedia of genes and genomes (KEGG) analysis. The GO and KEGG enrichment analyses were conducted using the R package 'clusterProfiler' to explore the differential signaling pathways and functions of the signature genes.

Machine learning algorithms. In the present study, two machine learning algorithms were applied to identify hub genes: LASSO to select important variables by shrinking the coefficients of less relevant genes to zero and SVM-RFE to identify core genes by iteratively removing less important features. To rigorously address potential overfitting, a nested cross-validation (CV) framework was implemented. Feature selection was performed by intersecting results from LASSO (via 'glmnet', 'lambda' selected by minimum mean squared error) and SVM-RFE (with linear kernel, 5 repeats of 10-fold CV) (23-26). The feature sets from both methods were intersected to obtain the final hub genes, which were visualized using a Venn diagram with the 'VennDiagram' R package (27).

GSEA. The 'c2.cp.kegg.v11.0. symbols' gene set from MSigDB was utilized as a reference for GSEA to investigate the biological significance of key genes. GSEA was performed using the 'clusterProfiler' R package, with visualization supported by the 'enrichplot' package. A significance threshold of corrected P<0.05 was established and 1,000 random sample alignments were employed to normalize enrichment scores.

Immune cell infiltration and its relationship with GRGs. Immune cell proportions were estimated using CIBERSORT (28,29) with 1,000 permutations, and only samples with P<0.05 were retained. Batch effects were corrected to minimize platform-related bias, and P-values were adjusted for multiple testing using the Benjamini-Hochberg method. Box-and-whisker plots were generated with the 'ggplot2' R package (30). To cross-validate the results, xCell (https://xcell.ucsf.edu/) and Estimating the Proportions of Immune and Cancer cells (https://github.com/GfellerLab/EPIC) methods were applied. Correlations between GRG expression and

Table I. Primer sequences for reverse transcription-quantitative PCR.

Gene	Forward (5'-3')	Reverse (3'-5')
LDHA	ACCGTGTTATTGGAAGCGGT	CTCCATGTTCCCCAAGGACC
TXN	GGTGAAGCAGATCGAGAGCA	CCACGTGGCTGAGAAGTCAA
GAPDH	TGTTGCCATCAATGACCCCT	TCGCCCCACTTGATTTTGGA

LDHA, lactate dehydrogenase A; *TXN*, thioredoxin.

immune cell fractions were calculated using the 'limma', 'dplyr', 'linkET' and 'ggplot2' packages. Differences across groups were assessed with the Wilcoxon test and visualization was performed using boxplots and principal component analysis (PCA) in 'ggplot2'.

Gene set variation analysis (GSVA). The 'c5.go.symbols' file and the 'c2.cp.kegg.symbols' file were procured from the GSVA section of the MSigDB database. Subsequently, the R packages 'GSVA' and 'limma' were employed to examine the altered pathways and biological functions (31,32) among the different clusters categorized by high and low expression levels of specific GRGs.

Construction of competing endogenous (ce)RNA regulatory networks. Databases, including miRanda algorithm (33,34), miRDB (https://mirdb.org/) and TargetScan (https://www.targetscan.org/), were used to predict the interactions between noncoding (nc)RNAs and mRNAs. In order to visualize and elucidate the interactions present within the ceRNA network, which encompasses long ncRNA-microRNA-mRNA interactions, Cytoscape (version 3.10.2; https://cytoscape.org/) was used to construct and visualize the network.

Validation of key genes in an independent cohort and nomogram construction. Candidate gene expression was further validated in an independent external cohort (GSE63085). After probe averaging with avereps(), the expression matrix was normalized using the limma package, and expression differences between control and LD samples were visualized and statistically compared. A logistic regression model based on the final key genes [lactate dehydrogenase A (LDHA) and thioredoxin (TXN)] was then established and visualized as a nomogram using the 'rms' package. Model performance was evaluated by receiver operating characteristic (ROC) analysis using 'pROC', and the area under the ROC curve (AUC) with 95% CI was estimated by 1,000 bootstrap resamples (35,36). Predicted probabilities were generated with plogis and shown in the nomogram (37). Model performance was evaluated by outer 5-fold cross-validation. Out-of-fold predictions were pooled for discrimination, calibration and decision curve analysis (DCA). Although an inner repeated 10-fold cross-validation scheme (3 repeats) was predefined, no further tuning or feature selection was performed because LDHA and TXN were fixed in advance. Performance was assessed by fold-specific AUCs, mean outer-fold AUC and pooled out-of-fold ROC with a bootstrap 95% CI. The final nomogram was fitted on the full dataset for visualization.

Experimental validation of key genes via reverse transcription-quantitative RT-qPCR. THP-1 human monocytic leukemia cells (ATCC TIB-202; American Type Culture Collection) were cultured in RPMI 1640 medium supplemented with 10% fetal bovine serum (cat. no. DT-500-S; DearyTech; official website: http://www.dearybio.cn/) and 1% antibiotic-antimycotic (cat. no. 15240062; Gibco; Thermo Fisher Scientific, Inc.) at 37˚C under 5% CO_2. For differentiation, the cells were plated and treated with 100 ng/ml phorbol 12-myristate 13-acetate for 24 h and then incubated overnight for the resting stage. Differentiated cells were subsequently infected with *Bb* strain B31 (ATCC 35210; American Type Culture Collection) at a multiplicity of infection of 0.1 or treated with vehicle control (PBS) for 24 h. Samples were collected and stored at -80˚C until processing. Total RNA was extracted using the MolPure® Cell/Tissue Total RNA Kit (cat. no. 19221ES50; Yeasen Biotechnology Co., Ltd.) according to the manufacturer's instructions. cDNA was then synthesized using the Hifair® III 1st Strand cDNA Synthesis SuperMix for qPCR (cat. no. 11141ES60; Yeasen Biotechnology Co., Ltd.) following the manufacturer's instructions. Quantitative real-time PCR was performed using the Gentier 96R System (Xi'an Tianlong Science and Technology Co., Ltd.) with Hieff UNICON® Universal Blue qPCR SYBR Master Mix (cat. no. 11184ES08; Yeasen Biotechnology Co., Ltd) according to the manufacturer's instructions, under the following conditions: 95˚C for 2 min; 40 cycles of 95˚C for 1 sec and 60˚C for 30 sec. GAPDH was used as the internal control. Gene expression was analyzed in three independent experiments via the $2^{-\Delta\Delta Cq}$ (38,39) method using primers designed by Tsingke Biotechnology (sequences shown in Table I).

Measurement of extracellular glucose (GLU) and lactate (LAC). Using the same THP-1 differentiation and Bb infection protocol described above, culture supernatants were collected for GLU and LAC measurement. GLU levels were determined using a GLU assay kit (cat. no. A154-1-1; Nanjing Jiancheng Bioengineering Institute), according to the manufacturer's instructions. LAC levels were measured using a Lactic Acid assay kit (cat. no. A019-2-2; Nanjing Jiancheng Bioengineering Institute), according to the manufacturer's instructions. For GLU measurement, 2.5 μl of each supernatant sample was added to a 96-well plate, followed by 200 μl of working solution, incubation at 37˚C for 10 min and absorbance measurement at 505 nm. For LAC measurement, 2.5 μl of each sample was added to a 96-well plate, followed by incubation with reagent 1 at 37˚C for 3 min and absorbance measurement at 546 nm (A1) using a microplate reader. Reagent 2 was then added,

followed by further incubation at 37˚C for 5 min and a second absorbance reading at 546 nm (A2) using a microplate reader. GLU and LAC concentrations were calculated according to the manufacturers' instructions.

Evaluation of applicant drugs. Drug molecules were identified using the Drug Signatures Database (DSigDB) through Enrichr, focusing on the key GRGs in the DEGs (40). Enrichr is a prominent web portal that features diverse gene set libraries for genome-wide gene set enrichment exploration (41). DSigDB functions as a global repository for identifying targeted drug substances associated with DEGs. The database comprises 22,527 gene sets. Access to DSigDB is facilitated via Enrichr under the Diseases/Drugs function (42). To strengthen the biological plausibility of the predicted drug-gene associations, cross-database validation was performed using multiple publicly available interaction resources, including the Comparative Toxicogenomics Database (CTD; https://ctdbase.org/), BioGRID (https://thebiogrid.org/), STRING (https://string-db.org/) and DrugBank (https://go.drugbank.com/).

Statistical analysis. Statistical analyses were used to determine data normality. For normally distributed data, an independent Student's t-test was used for comparison. For non-normally distributed data, the Mann-Whitney U-test was used for comparison. $P<0.05$ was considered to indicate a statistically significant difference between groups. Analyses and visualizations were performed using R (version 4.2.1) and GraphPad Prism (version 9.0.0; Dotmatics). The key analysis parameters and software package information are summarised in Table SIX.

Results

Expression profiles of GRGs in LD. To investigate the function of GRGs following Bb infection, their modified expression was comprehensively assessed using the GSE42606 database. The findings revealed significant alterations in the expression profiles of 63 GRGs, with 43 demonstrating upregulation in transcription and 20 exhibiting downregulation in expression (Fig. 2A). A list of the 63 significantly differentially expressed GRGs is provided in Table SII. A correlation analysis of these differentially expressed GRGs was simultaneously performed to examine their complex interactions (Fig. 2B). It became apparent that certain GRGs exhibit notable synergistic and antagonistic effects.

GO and KEGG analysis. The KEGG pathway analysis (Fig. 3A) of the 63 GRGs revealed significant enrichment in pathways such as 'Carbon metabolism', 'Glycolysis/Gluconeogenesis', 'Biosynthesis of amino acids' and the 'HIF-1 signaling pathway'. Enriched GO term analysis (Fig. 3B) highlighted the association of these genes with terms such as 'monosaccharide metabolic process' (GO:0005996), 'carbohydrate catabolic process' (GO:0016052) and 'pyridine nucleotide metabolic process' (GO:0019362). These findings suggest that there may be alterations in carbon metabolism in patients with LD compared with healthy individuals.

Machine learning algorithms. Considering the distinct differences between LD and controls, meaningful key genes were screened in the training dataset using two machine learning algorithms (LASSO and SVM-RFE) to differentiate Bb-infected samples. In the LASSO algorithm, 8 out of 63 GRGs were selected (Fig. 3C and D). Using the SVM-RFE algorithm, 14 GRGs were identified (maximum precision=0.957, minimum RMSE=0.0429) (Fig. 3E and F). Finally, the results of the two machine learning algorithms were combined with two genes identified as key genes (LDHA and TXN) (Fig. 3G).

GSEA of key genes. Because the potential function of key genes in LD is unknown, GSEA revealed their role and significance in LD. The first six pathways associated with the enrichment of their key genes (LDHA and TXN) are shown in Fig. 4A and B. The GSEA results indicated that LDHA-related genes were significantly enriched in several important pathways, including the 'chemokine signaling pathway', 'cytokine-cytokine receptor interaction' and 'lysosomes'. Similarly, TXN-related genes were significantly enriched in 'chemokine signaling', 'cytokine-cytokine receptor interactions' and 'graft-vs.-host disease' pathways. These findings highlight the involvement of LDHA and TXN in immune responses, intracellular signaling and inflammation-related processes.

GSVA. Subsequently, GSVA was performed using KEGG and GO gene sets to evaluate differences in pathway activity between the high- and low-expression groups. GSVA using KEGG gene sets revealed that no pathways were significantly enriched in the LDHA high-expression group compared to the low-expression group. However, multiple metabolic pathways had significantly lower enrichment scores. Specifically, 'Pantothenate and CoA biosynthesis', 'Biosynthesis of unsaturated fatty acids', 'Steroid biosynthesis' and 'Valine, leucine and isoleucine degradation' were downregulated. In addition, 'Amino sugar and nucleotide sugar metabolism' and glycosaminoglycan biosynthesis-related pathways, including 'Glycosaminoglycan biosynthesis-chondroitin sulfate/dermatan sulfate' and 'Glycosaminoglycan biosynthesis-heparan sulfate/heparin', were reduced. Several immune- and stress-related pathways, including the 'NOD-like receptor signaling pathway' and 'Apoptosis', also exhibited decreased enrichment (Fig. 5A). In the TXN high-expression group, KEGG analysis showed decreased enrichment in 'O-glycan biosynthesis' and the 'one-carbon pool by folate' compared to the low-expression group (Fig. 5B).

GO-based GSVA produced fewer and more heterogeneous signals, several of which were not readily interpretable in the PBMC context. Therefore, these results are provided in the Supplementary Materials and were not over-interpreted in the main text (Fig. S1).

Immune cell infiltration analysis. Employing CIBERSORT, the immunological disparities between the LD and control groups were examined. PCA revealed a striking non-overlapping configuration of elliptical clusters, illustrating distinct immune cell infiltration patterns between the LD and control groups (Fig. 6A). Comparative analysis revealed that, compared with the control cohort, the immunocellular landscape in the LD group showed elevated proportions of memory

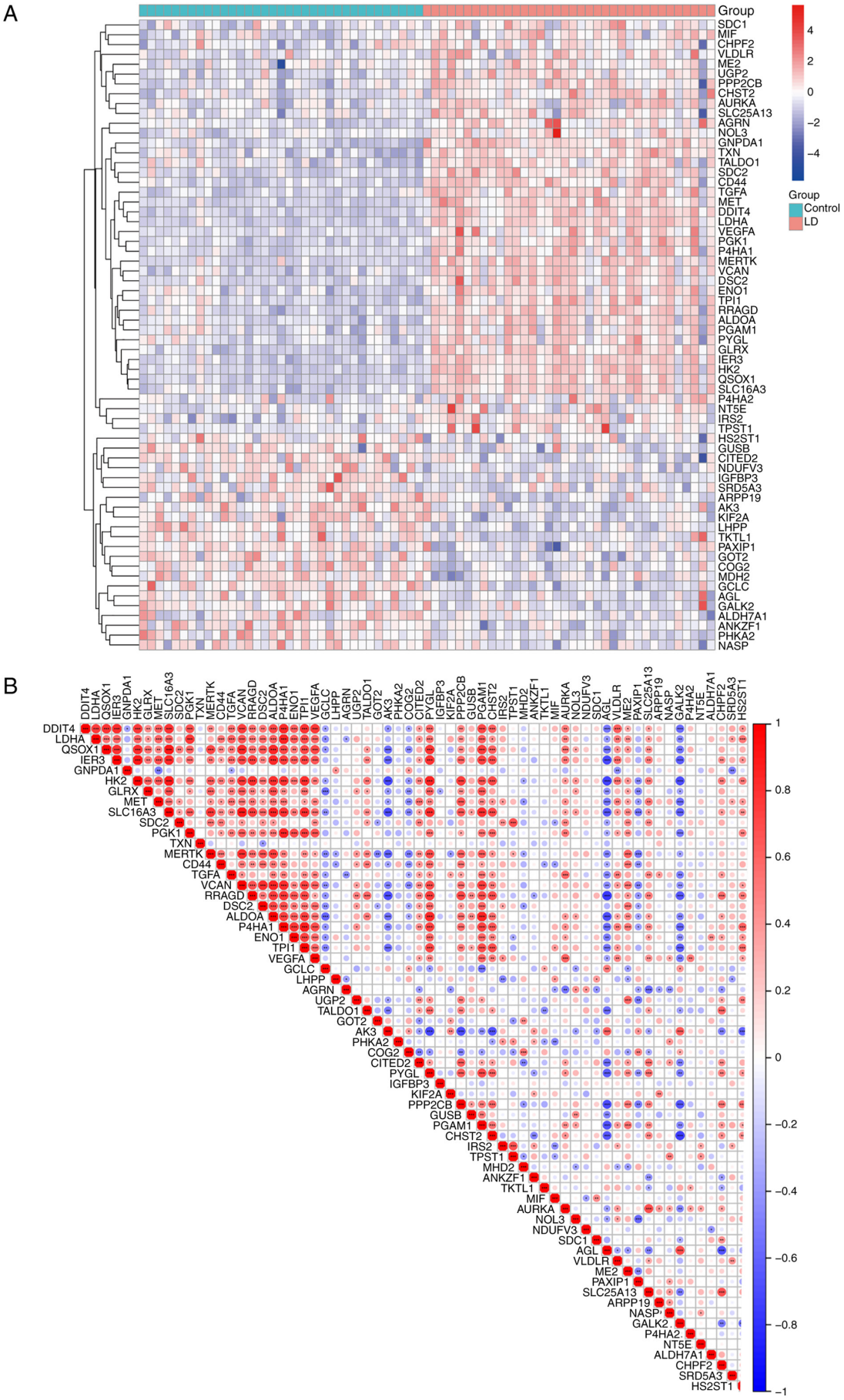

Figure 2. Analysis of expression levels of GRGs in LD. (A) Heat-map showing the expression pattern of GRGs in different samples. (B) Correlation heat map showing the correlation coefficients of the 63 GRGs. Red and green represent positive and negative correlations, respectively. *P<0.05, **P<0.01, ***P<0.001. GRGs, glycolysis-related genes; LD, lyme disease.

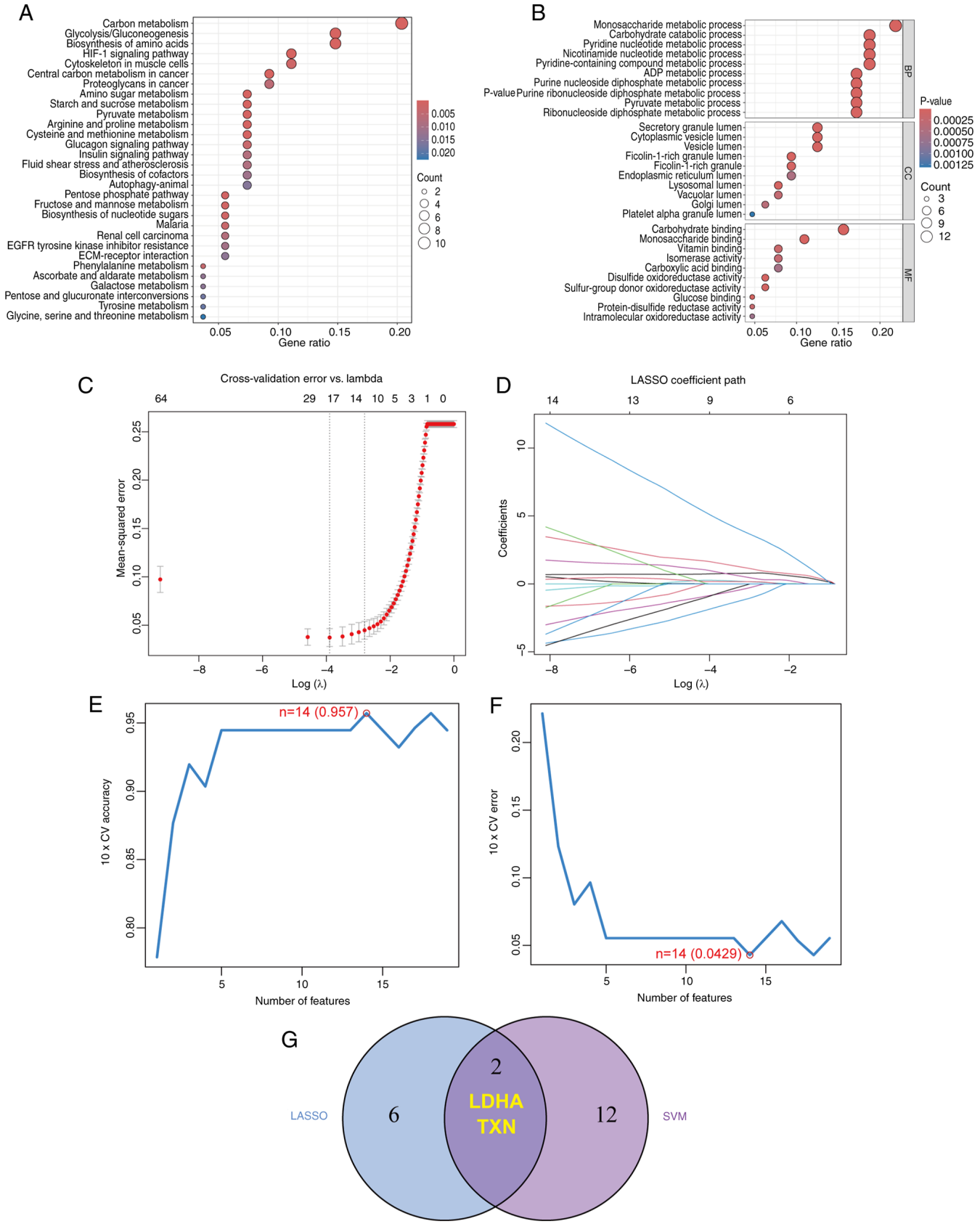

Figure 3. Enrichment analysis and machine learning approach reveals 2 genes in 63 GRGs were identified as key genes for LD. (A) KEGG term analysis of differentially expressed GRGs. (B) GO term analysis of differentially expressed GRGs. (C) ten-fold cross-validation curve for the LASSO logistic regression model used to determine the optimal penalty parameter. (D) coefficient profiles of candidate genes in the LASSO model as a function of log(λ). (E) Classification accuracy of the SVM-RFE model with different numbers of selected features. (F) Cross-validation error of the SVM-RFE model with different numbers of selected features. Finally, 14 genes (maximum precision=0.957, minimum root mean square error=0.0429) were identified as the best key genes; (G) The vein plot revealed two key gene regulation-related genes (LDHA and TXN) identified through LASSO and SVM-RFE methods. GRGs, glycolysis-related genes; LD, Lyme disease; GO, Gene Ontology; KEGG, Kyoto Encyclopedia of Genes and Genomes; LASSO, Least Absolute Shrinkage and Selection Operator; SVM-RFE, Support Vector Machine-Recursive Feature Elimination; CV, cross validation.

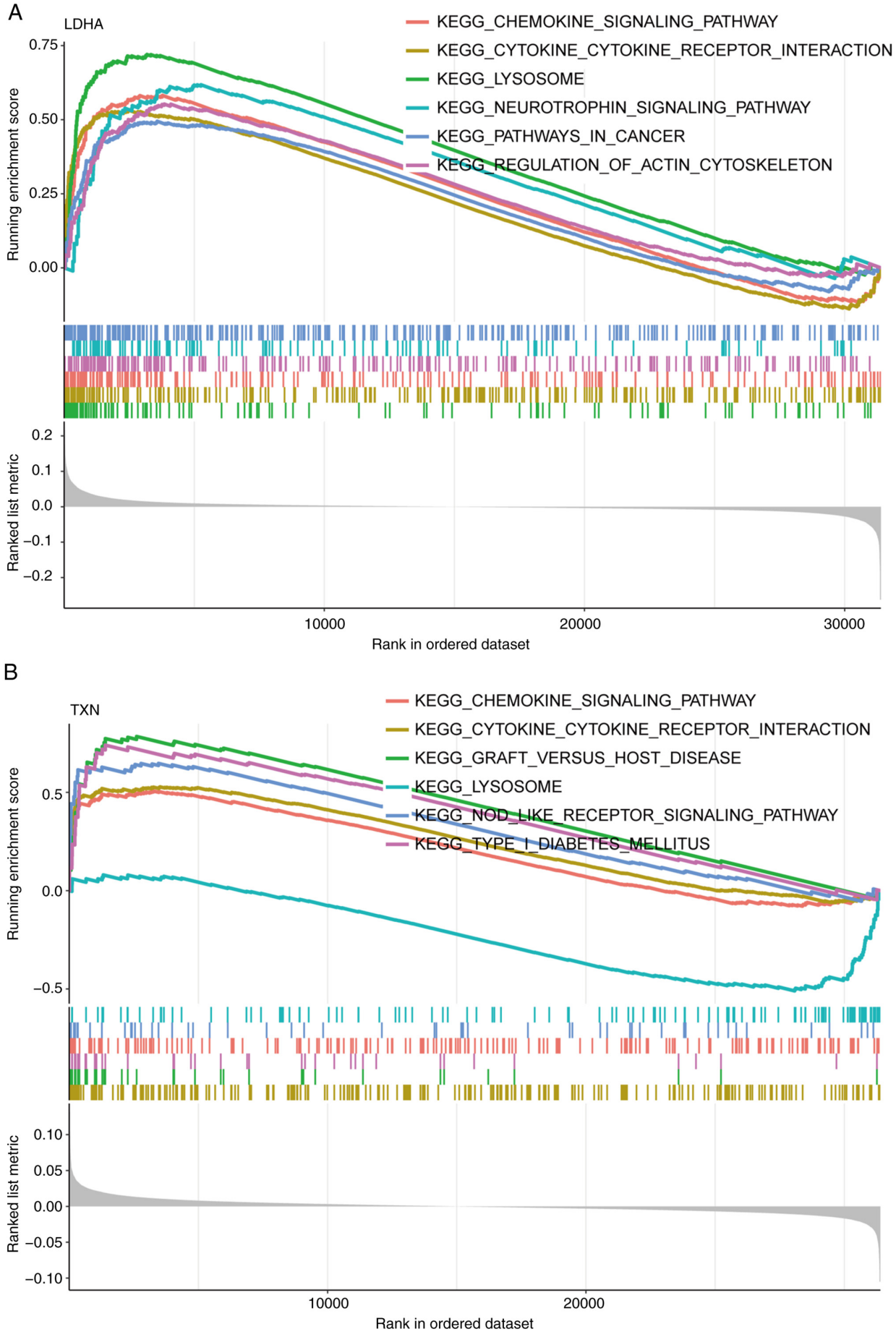

Figure 4. Single-gene GSEA-KEGG pathway analysis. GSEA-KEGG pathway analysis of (A) LDHA and (B) TXN. GSEA, Gene Set Enrichment Analysis; KEGG, Kyoto Encyclopedia of Genes and Genomes.

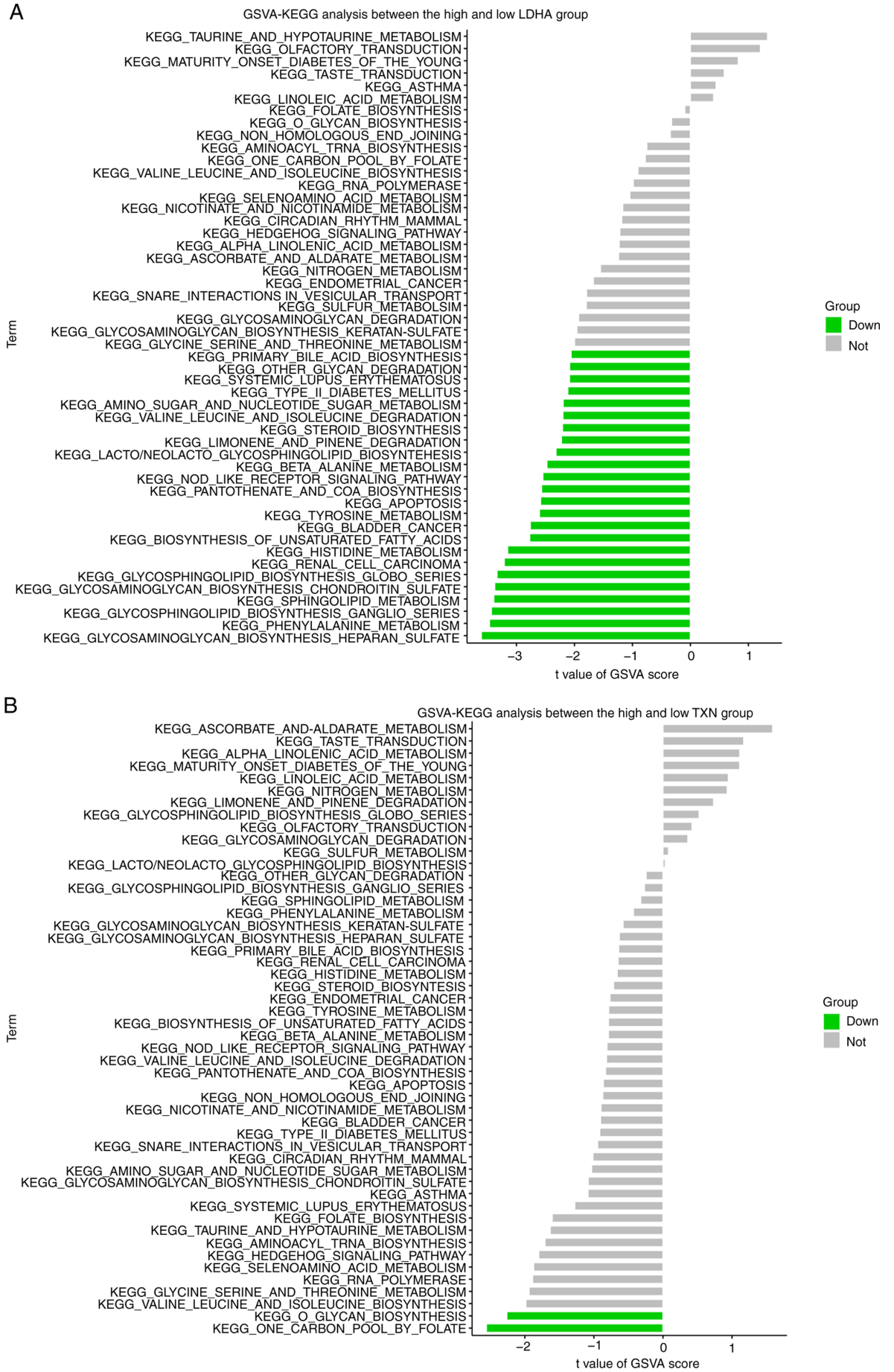

Figure 5. GSVA enrichment results based on KEGG. (A) GSVA results of the KEGG set in the LDHA high expressed group; (B) GSVA results of the KEGG set in the TXN high expressed group. GSVA, Gene Set Variation Analysis; KEGG, Kyoto Encyclopedia of Genes and Genomes.

B lymphocytes, regulatory T cells (Tregs), M0 macrophages, activated dendritic cells, activated mast cells and neutrophils. Conversely, the proportions of CD8+ T lymphocytes, resting memory CD4+ T cells, activated natural killer cells, M2 macrophages and resting mast cells were significantly lower in the LD cohort than those in the control group (Fig. 6B). The quality control filtering results for the CIBERSORT analysis are presented in Table SIII. The final immune cell composition data are provided in Table SIV. Furthermore, an in-depth investigation of the interrelationship between these pivotal characteristic genes and the immunological microenvironment was conducted. Notable findings included a strong positive correlation between LDHA and Tregs (r=0.33, P=0.05), a negative correlation with gamma delta T cells (r=-0.34, P=0.042) and a negative correlation with CD4 memory resting T cells (r=-0.4, P=0.016). TXN expression was significantly and negatively correlated with monocytes (r=-0.36, P=0.03) (Fig. 6C and D).

Drug-gene interaction network and cross-database validation of drug-gene interactions. To explore the potential therapeutic modulation of glycolytic dysregulation in LD, a drug-gene enrichment analysis was performed using DSigDB via the Enrichr platform. It is important to emphasize that these analyses were intended for hypothesis generation rather than direct therapeutic inference. A total of 6 candidate small molecules were identified based on the enrichment of the two hub genes (LDHA and TXN). The interaction network was visualized using Cytoscape (Fig. 7A). Fig. 7B shows the most effective drug. Detailed evidence of the cross-database interactions is provided in Table SV.

Hypothesis-generating ceRNA regulatory framework. To further explore the potential post-transcriptional regulatory mechanisms, a ceRNA network integrating the predicted lncRNA-miRNA-mRNA interactions was constructed using miRanda, miRDB and TargetScan. The network comprised 2 hub genes, 26 predicted miRNAs and 34 lncRNAs. This ceRNA framework is based solely on *in silico* target prediction and lacks matched miRNA and lncRNA expression data from the same PBMC cohort. Therefore, the current network can be regarded as a regulatory hypothesis map rather than a validated ceRNA axis (Fig. 7C).

Diagnostic modeling. A diagnostic prediction model for LD was created based on the hub genes LDHA and TXN in the training set (GSE42606). ROC curve analysis was conducted and the AUC values for LDHA and TXN were 0.975 and 0.934, respectively (Fig. 8A), indicating that both genes had strong diagnostic potential for LD. The diagnostic model based on these two genes showed robust performance, with an AUC of 0.974 (95% CI, 0.918-1.000) (Fig. 8B), demonstrating a strong predictive ability. Importantly, the LDHA-TXN logistic regression model retained good discriminative performance in the validation analysis-in the external validation set (GSE63085), the AUC values for LDHA and TXN were 0.826 and 0.874, respectively (Fig. 8C), ROC curve analysis was conducted, with an AUC of 0.879 (95% CI, 0.761-0.967) (Fig. 8D). Using case=1 as the positive class, the model achieved an accuracy of 0.805, a sensitivity of 0.857 and a specificity of 0.692. Detailed classification metrics are provided in Table SVI, with related analytical procedures and validation results described in Data S1, and detailed ROC analysis shown in Fig. S2.

Calibration curves confirmed that the nomogram accurately estimated the probability of robust host response to Bb exposure (Fig. 8E). The DCA further indicated that patients with LD could benefit from this nomogram (Fig. 8F). Detailed performance metrics are provided in Table SVII, whereas the related validation results and calibration/decision curve analyses are described separately in Data S1. A prediction model for diagnosing LD was developed using these trait genes, with each factor assigned a specific score, and a linear point axis was used to compute the total score associated with different levels of LD risk (Fig. 8G). Table SVIII shows the detailed coefficients of the 2-gene logistic regression diagnostic model.

Validation of key genes in an independent cohort. In the training set (GSE42606), the expression of LDHA was significantly higher in the disease group than that in the control group, whereas TXN showed significantly elevated expression in the disease group (Fig. 9A and B). To further validate these findings, the diagnostic performance of the model was tested using a validation set (GSE63085). In the validation set, LDHA and TXN showed significantly higher expression in LD samples than in controls (Fig. 9C and D).

Experimental validation of key gene expression by RT-qPCR. The expression levels of hub genes were also validated in THP-1 macrophages from both control and Bb-infected groups. The RT-qPCR results indicated that LDHA and TXN levels were significantly higher in the Bb-infected group than in the control group (Fig. 9E and F).

Glycolysis-related metabolic changes. To further verify whether Bb infection induced glycolytic changes in THP-1 cells, extracellular GLU and LAC levels were measured after Bb stimulation. Compared with the control group, Bb-infected THP-1 cells showed a decrease in extracellular GLU and a significant increase in LAC concentration in the supernatant (Fig. 9G and H).

Discussion

Glycolysis is a central metabolic pathway that provides energy to immune cells and plays a critical role in regulating immune responses and inflammation. Dysregulated glycolytic activity disrupts immune homeostasis and contributes to chronic inflammatory states (43-45). In addition, metabolic reprogramming of glycolysis is closely linked to macrophage polarization, with pro-inflammatory M1 macrophages primarily relying on glycolysis, whereas anti-inflammatory M2 macrophages depend more on oxidative phosphorylation (46-48). In the present study, 63 of the 200 GRGs were significantly altered following Bb infection, suggesting that host cells dynamically regulate glycolytic pathways during infection. Using the LASSO and SVM-RFE algorithms, two feature genes, LDHA and TXN, were further identified, which show transcriptional response signatures linked to Bb infection.

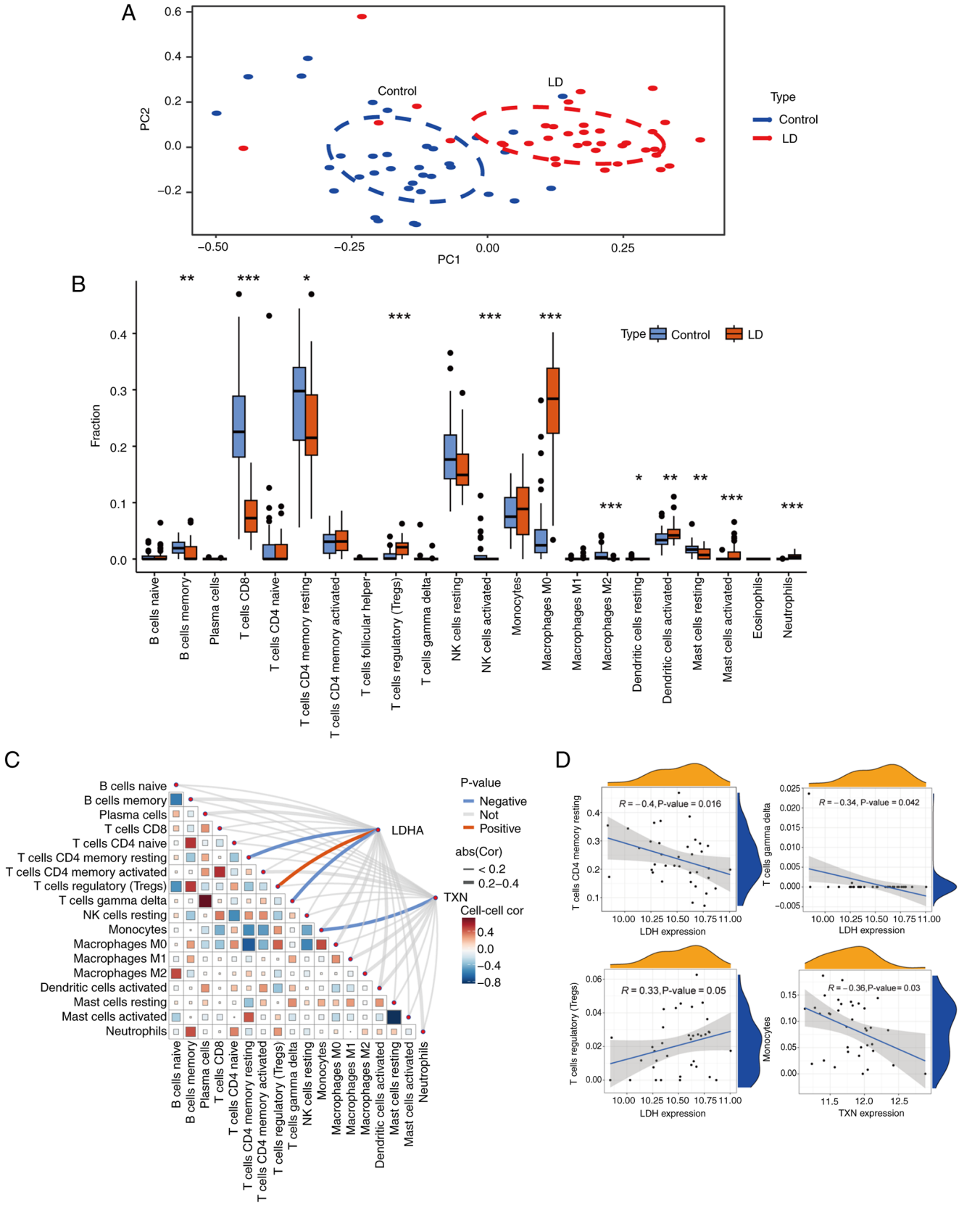

Figure 6. Results of the CIBERSORT analysis of the immune infiltration analysis. (A) PC analysis was performed between LD group and control group. Red points and ellipses indicate LD samples and blue points and ellipses indicate normal samples. (B) Box plot showing the significant difference in the infiltration of 22 immune cell types between the LD group and control group. (C) Correlation landscape of immune cell infiltration and its association with the key genes LDHA and TXN. The heatmap displays the Pearson correlation coefficients between the expression levels of 2 hub glycolysis-related differential genes (columns) and the infiltration levels of 22 immune cell types (rows) as determined by CIBERSORT analysis with the LM22 signature matrix. Red colors indicate positive correlations, while blue colors indicate negative correlations. Color intensity reflects the strength of correlation. (D) Representative scatter plots showing the correlations between the expression levels of LDHA/TXN and selected immune cell subsets, including resting memory CD4 T cells, gamma delta T cells, regulatory T cells and monocytes. Correlation coefficients and P-values are shown in each panel. *P<0.05, **P<0.01, ***P<0.001. PC, principal component; LD, Lyme disease.

A

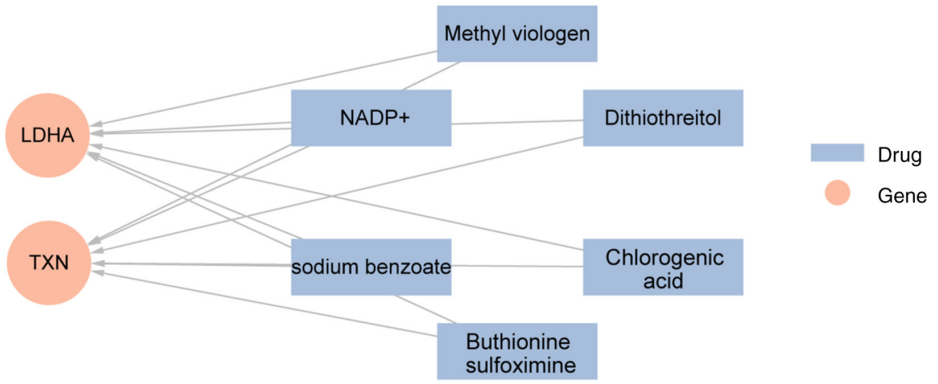

B

Name	Genes	Adjusted P-value	Molecular formula
Buthionine sulfoximine	LDHA and TXN	0.00078	$C_8H_{18}N_2O_3S$
Chlorogenic acid	LDHA and TXN	0.00078	$C_{16}H_{18}P_9$
NADP+	LDHA and TXN	0.00078	$C_{21}H_{28}N_7O_{17}P_3$
Methyl viologen	LDHA and TXN	0.00078	$C_{12}H_{14}N_2$
Dithiothreitol	LDHA and TXN	0.00078	$C_4H_{10}O_2S_2$
Sodium benzoate	LDHA and TXN	0.00078	$C_7H_5NaO_2$

C

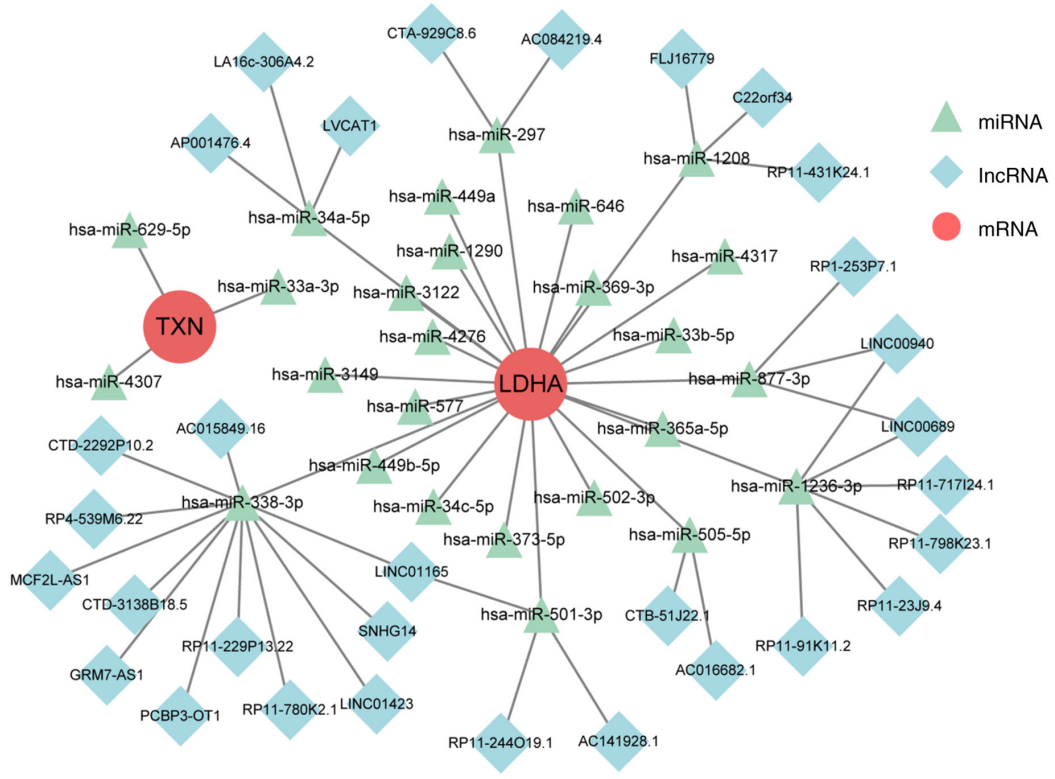

Figure 7. The candidate drug-gene interactions and ceRNA regulatory network construction. (A) Drug-gene interaction network constructed based on the Drug Gene Interaction Database. Red ellipse points represent genes and blue rectangle points represent drugs. (B) Predicted drug's molecular formula, gene and adjusted P-value. (C) A ceRNA regulatory network centered on 2 hub GRGs in Lyme disease. This focused sub-network illustrates the post-transcriptional regulation of 2 key GRGs through lncRNA-miRNA-mRNA interactions. Red ellipse represent mRNAs (LDHA and TXN), green triangles represent miRNAs (n=26) and blue diamonds represent lncRNAs (n=34). A total of 59 nodes and 60 edges are shown. Edge width represents the prediction confidence score from integrated analysis of the miRanda, miRDB and TargetScan databases. Network visualization was performed using Cytoscape v3.10.2 with a force-directed layout algorithm. crRNA, competing endogenous RNA; lncNRA, long non-coding RNA; miRNA, microRNAs; GRGs, glycolysis-related genes.

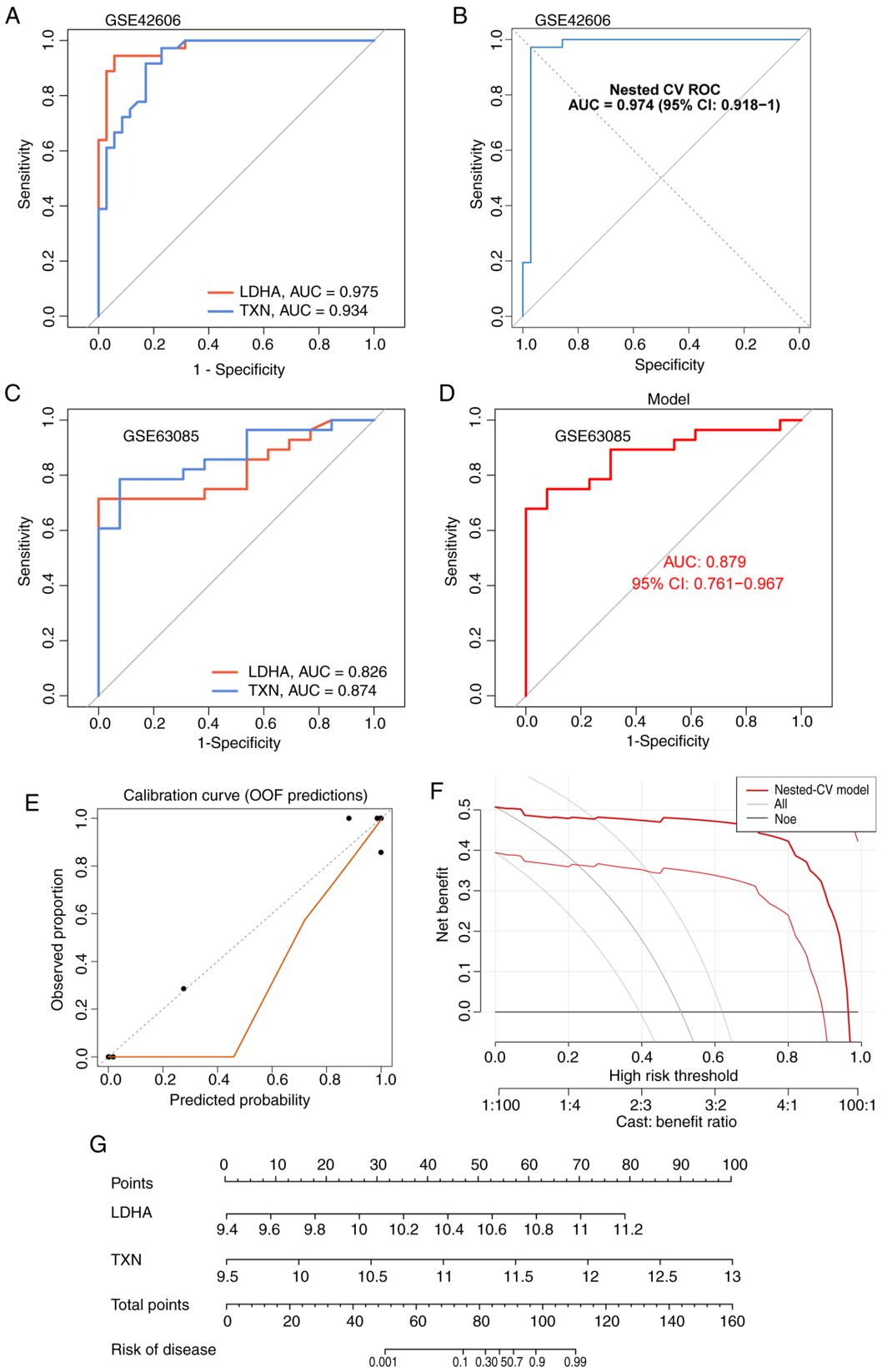

Figure 8. ROC curve, calibration plot and decision curve analysis of the LDHA-TXN model. (A) ROC curves of the two individual key genes, LDHA and TXN, in the GSE42606 cohort. The corresponding AUC values are shown in the panel. (B) ROC curve of the combined two-gene diagnostic model constructed using LDHA and TXN in the GSE42606 cohort. The AUC and 95% CI are indicated in the figure. (C) ROC curves of the individual genes LDHA and TXN in the independent validation cohort GSE63085, showing their diagnostic performance in external validation. (D) ROC curve of the combined two-gene diagnostic model in the independent validation cohort GSE63085. The AUC and 95% CI are shown in the panel. (E) Calibration curve of the nomogram/model. (F) DCA of the two-gene model. The red line represents the net benefit of the model, while the gray and black lines represent the strategies of treating all patients or none, respectively. (G) Nomogram constructed based on LDHA and TXN for individualized prediction of Lyme disease risk. In the nomogram, each variable corresponds to a score and the total score can be calculated by summing the scores of all variables. The ROC curve, calibration plot, and DCA shown were generated from pooled out-of-fold predictions obtained during outer 5-fold cross-validation, whereas the nomogram was fitted on the full dataset after validation for visualization only. ROC, receiver operating characteristic; AUC, area under curve; CV, cross-validation; DCA, decision curve analysis; OOF, out-of-fold.

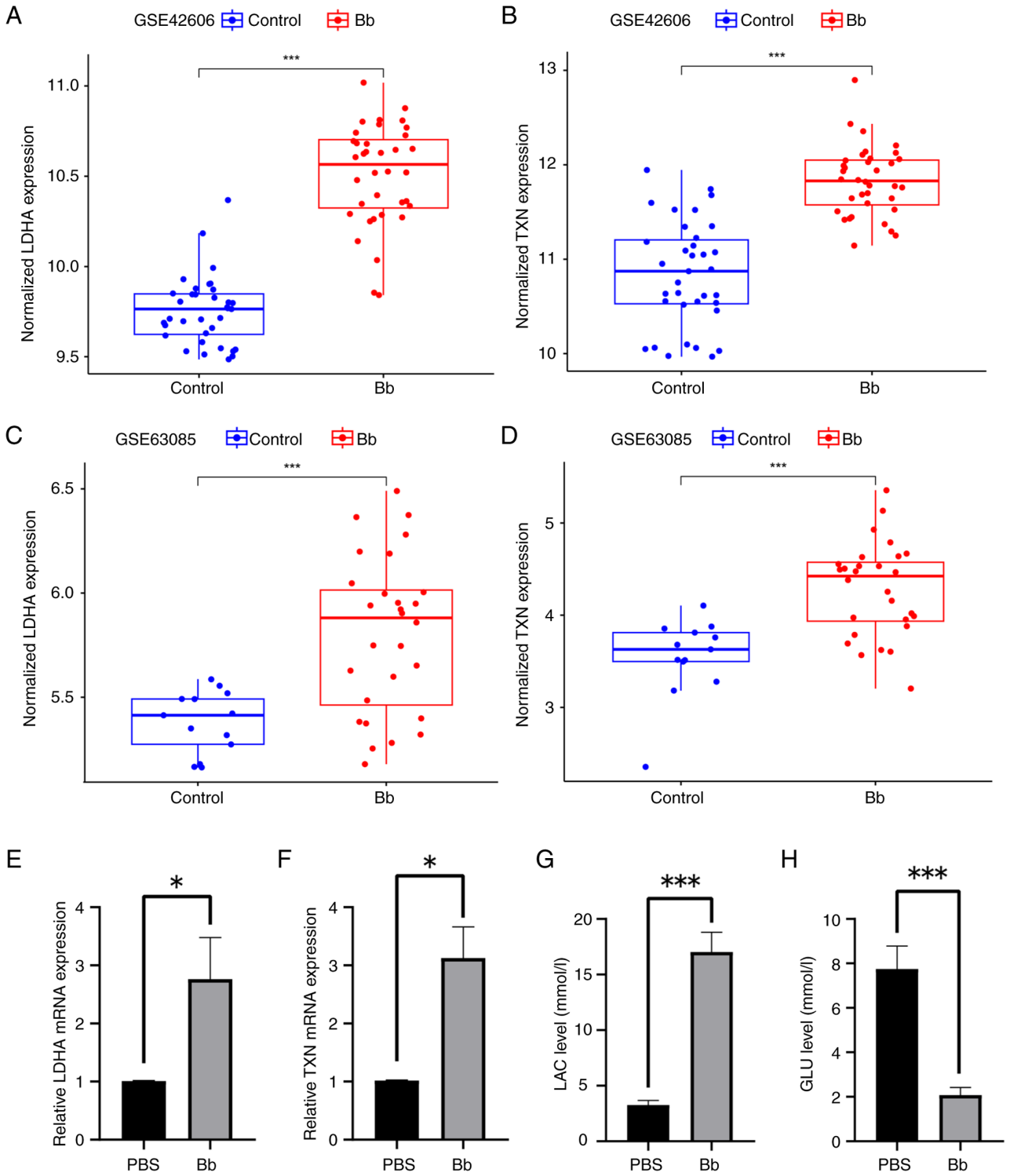

Figure 9. Validation of LDHA and TXN expression and glycolysis-related metabolic alterations in Lyme disease. Normalized expression levels of (A) LDHA and (B) TXN in the GSE42606 cohort between the control and Bb groups. Normalized expression levels of (C) LDHA and (D) TXN in the GSE63085 cohort between the control and Bb groups. Reverse transcription-quantitative PCR validation of (E) LDHA and (F) TXN mRNA expression in THP-1 cells after Bb stimulation compared with the PBS control group. (G) LAC and (H) GLU levels in culture supernatants of THP-1 cells after Bb stimulation and in the PBS control group. *P<0.05, ***P<0.001. LAC, lactate; GLU, extracellular glucose; Bb, *Borrelia burgdorferi*.

Previous studies have suggested that the pathophysiology of LD is significantly influenced by glycolysis (21), and constructing a predictive model based on GRGs is a promising approach to elucidate the etiology of LD and guide novel therapeutic strategies. In the present study, bioinformatics identified LDHA and TXN as key genes in the LD diagnostic model. Notably, beyond transcriptomic screening, it was observed that Bb infection was associated with reduced extracellular GLU and increased LAC production, providing experimental support that Bb infection is associated with glycolytic activation in host monocyte/macrophage-like cells. Within this framework, LDHA is mechanistically well aligned

with the observed phenotype, as it occupies a central position in LAC metabolism, glycolytic flux and immune regulation. Increased LDHA expression and elevated serum LAC levels have been observed in patients with Lyme borreliosis (18), and enhanced glycolytic activity in macrophages, accompanied by the upregulation of GRGs, including LDHA, suggests a role for metabolic reprogramming in the immune response to infection (49). Furthermore, Bb relies on its own lactate dehydrogenase (BbLDH) to maintain the $NADH/NAD^+$ balance, which is essential for bacterial survival and infectivity, and inhibition of BbLDH effectively suppresses pathogen growth (50). LDH has also been reported to inhibit growth *in vitro*, highlighting its central role in pathogen metabolism during LD (21). LDHA-driven glycolytic remodeling has also been linked to pro-inflammatory immune programs, including Th17-associated responses (51). By contrast, TXN is not a canonical glycolytic enzyme, but rather a redox regulator induced under infection and inflammatory stress (52-54). Its identification therefore suggests that the LD-associated transcriptional program extends beyond glycolysis itself and includes adaptive redox control. Consistent with this interpretation, GSEA revealed that both LDHA and TXN were associated with chemokine signaling and cytokine-cytokine receptor interaction pathways, which are central features of LD immunopathology (55-60). Together, these data support a model in which LDHA and TXN reflect two interconnected layers of the host response to Bb infection-metabolic activation and redox-inflammatory regulation-and may therefore serve as candidate biomarkers indicative of host response to Bb.

The relationship between diagnostic signature genes and immune cell infiltration was also examined. LDHA expression was positively correlated with Tregs and negatively correlated with γδ T cells and CD4 memory resting T cells, whereas TXN was negatively correlated with monocytes. These associations suggest that immune cell populations play a role in LD pathogenesis. Treg cells have been shown to mitigate arthritis symptoms (61,62), while γδ T cells are critical for promoting adaptive immune responses in Bb-infected mice, enhancing dendritic cell expression in lymph nodes and facilitating CD4+ T and B cell responses, thereby contributing to bacterial control and reduction of cardiac inflammation (63). Although direct evidence linking CD4 memory resting T cells to LD is lacking, multiple studies have reported that infection activates CD4+ T cells and promotes their migration to infected tissues to participate in inflammatory responses (64). Monocytes are directly activated by live Bb, inducing robust inflammatory responses including TNF-α, IL-6, IL-10 and IFN-β production, highlighting their role as key effector cells in LD immunity (65). Additionally, TXN can act as a chemotactic factor for monocytes, neutrophils and T cells, emphasizing its potential role in immune cell recruitment and regulation of inflammatory responses (52). Collectively, these findings suggest that LDHA and TXN may influence the pathogenesis of LD, partly by modulating immune cell infiltration.

Furthermore, these feature genes were analyzed by constructing a ceRNA network and predicting candidate drugs, thereby providing possible directions for future investigation of glycolysis-related regulatory mechanisms and immunotherapy for glycolytic abnormalities in LD. As both the drug-gene interaction analysis and ceRNA network construction were computationally inferred, a validation framework was proposed to improve translational relevance. First, an *in vitro* Bb infection model using THP-1-derived macrophages or primary PBMCs was established (51,55,62,66), followed by treatment with candidate drugs at graded concentrations. The key evaluation endpoints included inflammatory cytokine levels (67), glycolytic flux (9), LAC production (49) and changes in LDHA and TXN expression. Secondly, immune phenotype modulation can be assessed using macrophage polarization markers (68-70). Third, transcriptomic profiling after efficient drug treatment could determine whether the predicted glycolysis-immune axis is restored to a non-inflammatory state.

This study has several limitations. First, the present analyses were based on *ex vivo* peripheral PBMC stimulation models rather than on transcriptomic data from patients with clinical LD. As only a single 24-h time-point was examined, the identified two-gene signature likely reflects an early acute infection-related response rather than a definitive diagnostic model and may not be generalizable to chronic or late-stage LD. Secondly, several confounding factors should be considered. Inter-individual variation in the basal immune status of PBMC donors may have affected the stability of the machine learning models, whereas the public blood-derived datasets lacked sufficient geographical and ethnic diversity and did not capture localized immune features of affected tissues, such as skin or synovial fluid. Although correlations between these key genes and immune cell infiltration were observed, the underlying molecular mechanisms remain elusive. Finally, the present THP-1 experiments should be interpreted as preliminary monocyte-lineage validation of hub-gene expression trends. Further validation in primary cells and independent clinical cohorts will be an important direction of future work.

In conclusion, in the present study, the role of GRGs in LD was investigated. Bb infection induces significant alterations in host glycolytic gene expression, highlighting the importance of metabolic reprogramming in the immune response. Using integrated machine-learning analysis, two key feature genes, LDHA and TXN, were identified as having potential predictive value of Bb infection and were associated with immune infiltration. Abnormal immune cell infiltration was observed in PBMC following Bb infection, and the expression of these genes correlated with variations in immune cell proportions. In addition, several potential small-molecule candidates that target glycolytic dysregulation were identified. Collectively, these findings provide new insights into the metabolic-immune interactions underlying LD and may contribute to future diagnostic strategies and targeted therapeutic development.

Acknowledgements

The authors extend their sincere appreciation to Professor Yiqun Kuang for graciously facilitating access to the Biosafety Laboratory at the Research Center for Clinical Medicine within the First Affiliated Hospital of Kunming Medical University (Kunming, China).

Funding

The study was supported by the Yunnan Fundamental Research Projects (grant no. 202301BE070001-036) and the internal

projects of the First People's Hospital of Anning, affiliated with Kunming University of Science and Technology (grant nos. 2024AYY001 and 2024AYY005).

Availability of data and materials

The data generated in the present study may be requested from the corresponding author.

Authors' contributions

YD and YC contributed equally to this work. YD, YC and GZ conceived and designed the study. YL, ML, CS, XC, FY and QL performed the experiments and collected the data. YD, YC and YL analyzed and interpreted the data. YD and YC drafted the manuscript. GZ critically revised the manuscript and supervised the study. YD and GZ checked and confirmed the authenticity of the raw data. All authors have read and approved the final manuscript.

Ethics approval and consent to participate

Not applicable.

Patient consent for publication

Not applicable.

Competing interests

The authors declare that they have no competing interests.

References

1. Steere AC, Strle F, Wormser GP, Hu LT, Branda JA, Hovius JW, Li X and Mead PS: Lyme borreliosis. Nat Rev Dis Primers 2: 16090, 2016.
2. Kugeler KJ, Schwartz AM, Delorey MJ, Mead PS and Hinckley AF: Estimating the frequency of Lyme disease diagnoses, United States, 2010-2018. Emerg Infect Dis 27: 616-619, 2021.
3. Cardenas-de LGJ, De la Cruz-Valadez E, Ocampo-Candiani J and Welsh O: Clinical spectrum of Lyme disease. Eur J Clin Microbiol Infect Dis 38: 201-208, 2019.
4. Wormser GP, Ramanathan R, Nowakowski J, McKenna D, Holmgren D, Visintainer P, Dornbush R, Singh B and Nadelman RB: Duration of antibiotic therapy for early Lyme disease: A randomized double-blind placebo-controlled trial. Ann Intern Med 138: 697-704, 2003.
5. Bockenstedt LK, Gonzalez DG, Haberman AM and Belperron AA: Spirochete antigens persist near cartilage after murine Lyme borreliosis therapy. J Clin Invest 122: 2652-2660, 2012.
6. Williams MT, Zhang Y, Pulse ME, Berg RE and Allen MS: Suppression of host humoral immunity by *Borrelia burgdorferi* varies over the course of infection. Infect Immun 92: e00018, 2024.
7. Kraiczy P: Hide and seek: How Lyme disease spirochetes overcome complement attack. Front Immunol 7: 385, 2016.
8. Elsner RA, Hastey CJ, Olsen KJ and Baumgarth N: Suppression of long-lived humoral immunity following *Borrelia burgdorferi* infection. PLoS Pathog 11: e1004976, 2015.
9. Soto-Heredero G, Gómez DLHM, Gabandé-Rodríguez E, Oller J and Mittelbrunn M: Glycolysis: A key player in the inflammatory response. FEBS J 287: 3350-3369, 2020.
10. O'Neill LA and Pearce EJ: Immunometabolism governs dendritic cell and macrophage function. J Exp Med 213: 15-23, 2016.
11. Ye L, Jiang Y and Zhang M: Crosstalk between glucose metabolism, lactate production and immune response modulation. Cytokine Growth Factor Rev 68: 81-92, 2022.
12. Pearce EL and Pearce EJ: Metabolic pathways in immune cell activation and quiescence. Immunity 38: 643-643, 2013.
13. Buck MD, Sowell RT, Kaech SM and Pearce EL: Metabolic instruction of immunity. Cell 169: 570-586, 2017.
14. Pålsson-McDermott EM and O'Neill L: Targeting immunometabolism as an anti-inflammatory strategy. Cell Res 30: 300-314, 2020.
15. Kornberg MD, Bhargava P, Kim PM, Putluri V, Snowman AM, Putluri N, Calabresi PA and Snyder SH: Dimethyl fumarate targets GAPDH and aerobic glycolysis to modulate immunity. Science 360: 449-453, 2018.
16. Shirai T, Nazarewicz RR, Wallis BB, Yanes RE, Watanabe R, Hilhorst M, Tian L, Harrison DG, Giacomini JC, Assimes TL, *et al*: The glycolytic enzyme PKM2 bridges metabolic and inflammatory dysfunction in coronary artery disease. J Exp Med 213: 337-354, 2016.
17. Peng M, Yin N, Chhangawala S, Xu K, Leslie CS and Li MO: Aerobic glycolysis promotes T helper 1 cell differentiation through an epigenetic mechanism. Science 354: 481-484, 2016.
18. Oosting M, Kerstholt M, Ter Horst R, Li Y, Deelen P, Smeekens S, Jaeger M, Lachmandas E, Vrijmoeth H, Lupse M, *et al*: Functional and genomic architecture of *Borrelia burgdorferi*-induced cytokine responses in humans. Cell Host Microbe 20: 822-833, 2016.
19. Kim TK, Tirloni L, Bencosme-Cuevas E, Kim TH, Diedrich JK, Yates JR and Mulenga A: *Borrelia burgdorferi* infection modifies protein content in saliva of *Ixodes scapularis* nymphs. BMC Genomics 22: 152, 2021.
20. Corona A and Schwartz I: *Borrelia burgdorferi*: Carbon metabolism and the tick-mammal enzootic cycle. Microbiol Spectr 3: 10, 2015.
21. Lynch A, Pearson P, Savinov SN, Li AY and Rich SM: Lactate dehydrogenase inhibitors suppress *Borrelia burgdorferi* growth in vitro. Pathogens 12: 962, 2023.
22. Ritchie ME, Phipson B, Wu D, Hu Y, Law CW, Shi W and Smyth GK: limma powers differential expression analyses for RNA-sequencing and microarray studies. Nucleic Acids Res 43: e47, 2015.
23. Tibshirani R: Regression shrinkage selection via the LASSO. J R Stat Soc Series B Stat Methodol 73: 273-282, 2011.
24. Sauerbrei W, Royston P and Binder H: Selection of important variables and determination of functional form for continuous predictors in multivariable model building. Stat Med 26: 5512-5528, 2007.
25. Guyon I, Weston J, Barnhill S and Vapnik V: Gene selection for cancer classification using support vector machines. Mach Learn 46: 389-422, 2002.
26. Lewis MJ, Spiliopoulou A, Goldmann K, Pitzalis C, McKeigue P and Barnes MR: nestedcv: An R package for fast implementation of nested cross-validation with embedded feature selection designed for transcriptomics and high-dimensional data. Bioinform Adv 3: vbad048, 2023.
27. Chen H and Boutros PC: VennDiagram: A package for the generation of highly customizable Venn and Euler diagrams in R. BMC Bioinformatics 12: 35, 2011.
28. Aran D, Hu Z and Butte AJ: xCell: Digitally portraying the tissue cellular heterogeneity landscape. Genome Biol 18: 220, 2017.
29. Aran D: Cell-type enrichment analysis of bulk transcriptomes using xCell. Methods Mol Biol 2120: 264-276, 2020.
30. Gustavsson EK, Zhang D, Reynolds RH, Garcia-Ruiz S and Ryten M: ggtranscript: An R package for the visualization and interpretation of transcript isoforms using ggplot2. Bioinformatics 38: 3844-3846, 2022.
31. Hänzelmann S, Castelo R and Guinney J: GSVA: Gene set variation analysis for microarray and RNA-seq data. BMC Bioinformatics 14: 7, 2013.
32. Lin Y, Liang R, Ye J, Li Q, Liu Z, Gao X, Piao X, Mai R, Zou D and Ge L: A twenty gene-based gene set variation score reflects the pathological progression from cirrhosis to hepatocellular carcinoma. Aging (Albany NY) 11: 11157-11169, 2019.
33. Betel D, Wilson M, Gabow A, Marks DS and Sander C: The microRNA.org resource: Targets and expression. Nucleic Acids Res 36: D149-D153, 2008.
34. John B, Enright AJ, Aravin A, Tuschl T, Sander C and Marks DS: Human MicroRNA targets. PLoS Biol 2: e363, 2004.
35. Mandrekar JN: Receiver operating characteristic curve in diagnostic test assessment. J Thorac Oncol 5: 1315-1316, 2010.
36. Robin X, Turck N, Hainard A, Tiberti N, Lisacek F, Sanchez JC and Müller M: pROC: An open-source package for R and S+ to analyze and compare ROC curves. BMC Bioinformatics 12: 77, 2011.

37. Pajouheshnia R, Pestman WR, Teerenstra S and Groenwold RHH: A computational approach to compare regression modelling strategies in prediction research. BMC Med Res Methodol 16: 107, 2016.
38. Livak KJ and Schmittgen TD: Analysis of relative gene expression data using real-time quantitative PCR and the 2(-Delta Delta C(T)) method. Methods 25: 402-408, 2001.
39. Schmittgen TD and Livak KJ: Analyzing real-time PCR data by the comparative C(T) method. Nat Protoc 3: 1101-1108, 2008.
40. Yoo M, Shin J, Kim J, Ryall KA, Lee K, Lee S, Jeon M, Kang J and Tan AC: DSigDB: Drug signatures database for gene set analysis. Bioinformatics 31: 3069-3071, 2015.
41. Kuleshov MV, Jones MR, Rouillard AD, Fernandez NF, Duan Q, Wang Z, Koplev S, Jenkins SL, Jagodnik KM, Lachmann A, *et al*: Enrichr: A comprehensive gene set enrichment analysis web server 2016 update. Nucleic Acids Res 44: W90-W97, 2016.
42. Keenan AB, Jenkins SL, Jagodnik KM, Koplev S, He E, Torre D, Wang Z, Dohlman AB, Silverstein MC, Lachmann A, *et al*: The library of integrated network-based cellular signatures NIH program: System-level cataloging of human cells response to perturbations. Cell Syst 6: 13-24, 2018.
43. Tannahill GM, Curtis AM, Adamik J, Palsson-McDermott EM, McGettrick AF, Goel G, Frezza C, Bernard NJ, Kelly B, Foley NH, *et al*: Succinate is an inflammatory signal that induces IL-1β through HIF-1α. Nature 496: 238-242, 2013.
44. Palsson-McDermott EM, Curtis AM, Goel G, Lauterbach MAR, Sheedy FJ, Gleeson LE, van den Bosch MW, Quinn SR, Domingo-Fernandez R, Johnston DG *et al*: Pyruvate kinase M2 regulates HIF-1α activity and IL-1β induction and is a critical determinant of the Warburg effect in LPS-activated macrophages. Cell Metab 21: 65-80, 2015.
45. O'Neill LA, Kishton RJ and Rathmell J: A guide to immunometabolism for immunologists. Nat Rev Immunol 16: 553-565, 2016.
46. Martínez-Reyes I and Chandel NS: Mitochondrial TCA cycle metabolites control physiology and disease. Nat Commun 11: 102, 2020.
47. Chen S, Xu Y, Zhuo W and Zhang L: The emerging role of lactate in tumor microenvironment and its clinical relevance. Cancer Lett 590: 216837, 2024.
48. Viola A, Munari F, Sánchez-Rodríguez R, Scolaro T and Castegna A: The metabolic signature of macrophage responses. Front Immunol 10: 1462, 2019.
49. Barriales D, Martín-Ruiz I, Carreras-González A, Montesinos-Robledo M, Azkargorta M, Iloro I, Escobés I, Martín-Mateos T, Atondo E, Palacios A, *et al*: *Borrelia burgdorferi* infection induces long-term memory-like responses in macrophages with tissue-wide consequences in the heart. PLoS Biol 19: e3001062, 2021.
50. Sze CW, Lynch MJ, Zhang K, Neau DB, Ealick SE, Crane BR and Li C: Lactate dehydrogenase is the Achilles' heel of Lyme disease bacterium *Borreliella burgdorferi*. mBio 16: e037284, 2025.
51. Dai M, Wang L, Yang J, Chen J, Dou X, Chen R, Ge Y and Lin Y: LDHA as a regulator of T cell fate and its mechanisms in disease. Biomed Pharmacother 158: 114164, 2023.
52. Bertini R, Howard OM, Dong HF, Oppenheim JJ, Bizzarri C, Sergi R, Caselli G, Pagliei S, Romines B, Wilshire JA, *et al*: Thioredoxin, a redox enzyme released in infection and inflammation, is a unique chemoattractant for neutrophils, monocytes and T cells. J Exp Med 189: 1783-1789, 1999.
53. Li B, Ming H, Qin S, Nice EC, Dong J, Du Z and Huang C: Redox regulation: Mechanisms, biology and therapeutic targets in diseases. Signal Transduct Target Ther 10: 72, 2025.
54. Dagah OMA, Silaa BB, Zhu M, Pan Q, Qi L, Liu X, Liu Y, Peng W, Ullah Z, Yudas AF, *et al*: Exploring immune redox modulation in bacterial infections: Insights into thioredoxin-mediated interactions and implications for understanding host-pathogen dynamics. Antioxidants (Basel) 13: 545, 2024.
55. Shin JJ, Strle K, Glickstein LJ, Luster AD and Steere AC: *Borrelia burgdorferi* stimulation of chemokine secretion by cells of monocyte lineage in patients with Lyme arthritis. Arthritis Res Ther 12: R168, 2010.
56. Botey-Bataller J, Vrijmoeth HD, Ursinus J, Kullberg BJ, van den Wijngaard CC, Ter Hofstede H, Alaswad A, Gupta MK, Roesner LM, Huehn J, *et al*: A comprehensive genetic map of cytokine responses in Lyme borreliosis. Nat Commun 15: 3795, 2024.
57. Lu Y, Osis G, Zmijewska AA, Traylor A, Thukral S, Wilson L, Barnes S, George JF and Agarwal A: Macrophage-specific lactate dehydrogenase expression modulates inflammatory function in vitro. Kidney360 6: 197-207, 2025.
58. Song YJ, Kim A, Kim GT, Yu HY, Lee ES, Park MJ, Kim YJ, Shim SM and Park TS: Inhibition of lactate dehydrogenase A suppresses inflammatory response in RAW 264.7 macrophages. Mol Med Rep 19: 629-647, 2019.
59. Qayyum N, Haseeb M, Kim MS and Choi S: Role of thioredoxin-interacting protein in diseases and its therapeutic outlook. Int J Mol Sci 22: 2754, 2021.
60. Nakamura H, Herzenberg LA, Bai J, Araya S, Kondo N, Nishinaka Y, Herzenberg LA and Yodoi J: Circulating thioredoxin suppresses lipopolysaccharide-induced neutrophil chemotaxis. Proc Natl Acad Sci USA 98: 15143-15148, 2001.
61. Mason LM, Veerman CC, Geijtenbeek TB and Hovius JW: Menage a trois: Borrelia, dendritic cells and tick saliva interactions. Trends Parasitol 30: 95-103, 2014.
62. Shen S, Shin JJ, Strle K, McHugh G, Li X, Glickstein LJ, Drouin EE and Steere AC: Treg cell numbers and function in patients with antibiotic-refractory or antibiotic-responsive Lyme arthritis. Arthritis Rheum 62: 2127-2137, 2010.
63. Shi C, Sahay B, Russell JQ, Fortner KA, Hardin N, Sellati TJ and Budd RC: Reduced immune response to *Borrelia burgdorferi* in the absence of γδ T cells. Infect Immun 79: 3940-3946, 2011.
64. Tracy KE and Baumgarth N: *Borrelia burgdorferi* manipulates innate and adaptive immunity to establish persistence in rodent reservoir hosts. Front Immunol 8: 116, 2017.
65. Salazar JC, Duhnam-Ems S, La Vake C, Cruz AR, Moore MW, Caimano MJ, Velez-Climent L, Shupe J, Krueger W and Radolf JD: Activation of human monocytes by live *Borrelia burgdorferi* generates TLR2-dependent and independent responses including induction of IFN-β. PLoS Pathog 5: e1000444, 2009.
66. Stokes JV, Moraru GM, McIntosh C, Kummari E, Rausch K and Varela-Stokes AS: Differentiated THP-1 cells exposed to pathogenic and nonpathogenic *Borrelia* species demonstrate minimal differences in production of inflammatory cytokines. Vector Borne Zoonotic Dis 16: 691-695, 2016.
67. Strle K, Drouin EE, Shen S, El Khoury J, McHugh G, Ruzic-Sabljic E, Strle F and Steere AC: *Borrelia burgdorferi* stimulates macrophages to secrete higher levels of cytokines and chemokines than *Borrelia afzelii* or *Borrelia garinii*. J Infect Dis 200: 1936-1943, 2009.
68. Lasky CE, Olson RM and Brown CR: Macrophage polarization during murine Lyme borreliosis. Infect Immun 83: 2627-2645, 2015.
69. Akinlusi I, Kan B, Shi T, Barragan J, Bouchot C and Cervantes J: Human microglia polarization following infection with the Lyme disease spirochete. J Investig Med 73: 172-178, 2025.
70. Woitzik P and Linder S: Molecular mechanisms of *Borrelia burgdorferi* phagocytosis and intracellular processing by human macrophages. Biology (Basel) 10: 567, 2021.